

Surface modification of nylon 6 by 50 Hz dielectric barrier discharge produced in air and argon at atmospheric pressure

Bikash Shrestha¹, Rajesh Prakash Guragain^{1,*}, Binita Sedhai¹
Hom Bahadur Baniya², Ujjwal Man Joshi¹, Deepak Prasad Subedi¹

¹Department of Physics, School of Science, Kathmandu University, Dhulikhel, Kavre

²Department of Physics, Amrit Campus, Tribhuvan University, Kathmandu, Nepal

*Corresponding author. Email: rayessprakash@gmail.com

Abstract

This paper reports the use of dielectric barrier discharge (15.65 kV, 50 Hz) produced in an air and argon environment at atmospheric pressure to modify the surface of Nylon 6. Power dissipation in air and argon DBD was determined to be 14.60 W and 12.00 W, respectively. Similarly, the average density and temperature of an electron in air DBD were found to be $1.74 \times 10^{11} \text{ cm}^{-3}$ and 1.31 eV, respectively, while the values were $2.50 \times 10^{11} \text{ cm}^{-3}$ and 0.68 eV in argon DBD. The water contact angle (WCA) was measured to confirm the enhancement in wettability. On treating the sample with air DBD for 15 minutes, the contact angle reduced from $134.07^\circ \pm 3.20^\circ$ to $89.11^\circ \pm 3.06^\circ$ while it was reduced to $82.74^\circ \pm 4.20^\circ$ within 1 minute using argon. The study found that treating a hydrophobic sample of Nylon 6 with DBD for a certain period of time transformed it into a hydrophilic one, and extending the treatment time further enhanced its wettability. The use of argon DBD was found to be more effective than air DBD in altering the surface properties of the sample, as the sample became hydrophilic after only one minute of treatment with argon DBD and completely wettable after three minutes. The findings suggest that air and argon DBD have potential applications in modifying the surface properties of Nylon 6, which could have practical implications in the production of textiles, membranes, and other materials.

Keywords

Dielectric Barrier Discharge (DBD), Electron density, Lissajous figure, Nylon 6, Polymer, Surface modification, Water contact angle (WCA).

Article information

Manuscript received: May 18, 2022; Accepted: April 26, 2023

DOI <https://doi.org/10.3126/bibechana.v20i2.45159>

This work is licensed under the Creative Commons CC BY-NC License. <https://creativecommons.org/licenses/by-nc/4.0/>

1 Introduction

Polymers have aided in the growth of technology, applied engineering, and materials science due to their remarkable material characteristics [1]. How-

ever, polymers are frequently inappropriate for use in their pristine state as they are resistant to biological and chemical agents [2, 3]. They have low surface energy, poor wettability, printability, and other technologically significant aspects [4, 5]. As

a result, surface treatment is needed to transform them into more sophisticated materials for use in many commercial applications [6]. To modify polymer surfaces, a variety of surface treatments are available, ranging from large-scale treatments to precision ones [7]. Plasma treatment is one of the commonly used precise treatments as it has the ability to selectively alter the chemical and physical features of the polymer surfaces without changing their fundamental bulk properties. Further, plasma treatment is resource-efficient, environmentally friendly, and treatment time is comparatively shorter [8–12]. McCord used atmospheric pressure plasmas to modify nylon fabrics and demonstrated that modification can be done without affecting the bulk properties [13]. Swar et al. showed that due to the presence of amine groups, the surface of treated Nylon 6 films was likely to be bio-compatible for future medical applications [14]. Thomson et al. found a reduction in the concentration of oxygen in the treated surface was the main cause of the decrease in the wettability of the sample with an increase in treatment time [15]. In recent years, Nylon 6 polymers have been in high demand, such as in biomedical and industrial applications. In this study, non-thermal plasma at atmospheric pressure is generated through dielectric barrier discharge at 50 Hz frequency in air and argon environment. Two methods: electrical and optical are used for plasma diagnostics. The water contact angle and surface free energy of samples before and after treatment were measured to study the considerable changes in the surface properties of the treated sample.

2 Experimental Methods

2.1 Nylon 6 sample

Nylon 6, also known as polycaprolactam or polyamide 6, is a synthetic polymer made up of a monomer, caprolactam [16, 17]. The Nylon 6 sample used in this study is shown in Figure 1. The thickness of the sample is 0.32 mm and is yellow in color. The dimension of the sample used throughout the study was 2.5 cm × 2.5 cm.

2.2 Experimental set-up

Figure 2 shows the experimental set-up of circular parallel plate electrode DBD system. The system comprises of a transparent, cylinder-shaped polycarbonate reactor that is 10 cm in diameter, 10 cm

in height, and 0.5 cm thick. Two circular brass electrodes of identical shape and size, each measuring 5.1 cm in diameter and 1.0 cm in thickness, are placed one on top of the other in the reactor, with a suitable gap between them. The upper electrode can be moved up and down on the vertical scale to adjust the electrode gap, whereas the lower electrode is fixed. A circular polycarbonate plate having a diameter of 9.7 cm and a thickness of 0.2 cm covering the lower electrode acts as a dielectric barrier. This inhibits the formation of arc discharges. The upper electrode is connected in series to the high ac power supply through a ballast resistor (20 M Ω , 2 W). The high tension to low tension ratio (HT/LT) of the step-up transformer used is 78.26. The lower electrode is grounded through the shunt resistance (10 K Ω , 10 W). The spacing between the electrodes had been maintained at 0.35 cm throughout the research study.

2.3 Electrical and optical diagnostics

One should also be familiar with the properties of the plasma being used. A well-defined insight into some quantities that describe plasma state is needed to understand plasma properties. The most elemental quantities are electron density and electron temperature. These quantities are known as plasma parameters. The most tempting feature of a plasma diagnostic approach is that it is non-invasive [18].

For electrical and optical diagnostics, an oscilloscope probe (Kenwood PC-54 oscilloscope probe) is used to measure discharge current across shunt resistor. The voltage across the electrode is measured through a high-voltage probe (PINTEK HVP-28 HF). Both the high-voltage probe and the oscilloscope probe are connected to the input channel of the digital oscilloscope (Tektronix TDS 2002) which records and displays voltage and current waveforms as a function of time. A small hole is drilled into the top circular base of the polycarbonate cylinder to allow the inlet of argon gas. The gas flow rate of argon was maintained at 2 L/min. A small hole is also drilled in the middle of the lateral surface of the polycarbonate cylinder, just opposite the electrode gap, for the insertion of fiber optical cable. The Ocean Optics USB2000+ Fiber Optic Spectrometer is used to take optical spectra for optical characterization. Figure 3 shows the photograph of the DBD system used in this research work.



Figure 1: Nylon 6 sample of dimension 2.5 cm \times 2.5 cm.

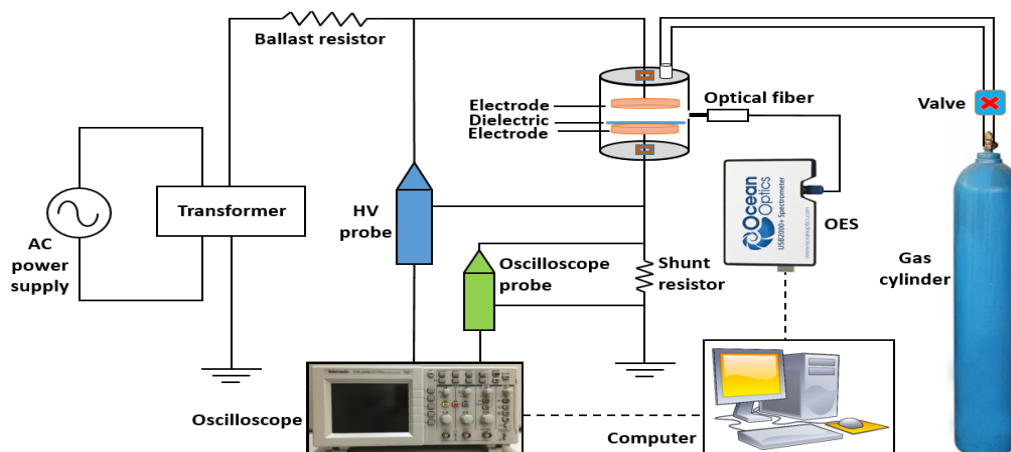


Figure 2: Schematic diagram of the experimental set-up.

3 Results and Discussion

sure [19].

3.1 Electrical Characterization

Figure 4 shows the variation of applied voltage and discharge current of air and argon DBD as a function of time. The applied voltage is sinusoidal in nature while the current signal consists of significant number of individual non-uniform filaments referred to as micro-discharges. DBD generally has several non-uniform filaments at atmospheric pres-

3.2 Electrical Diagnostics

A standard approach for electrical diagnostics of DBD discharges is the Lissajous figure. The charge-voltage (Q-V) loop is commonly known as the Lissajous figure. The power dissipated, average electron density, etc., parameters can be found from Lissajous figures as a function of several parameters [20, 21].



Figure 3: Photograph of DBD system.

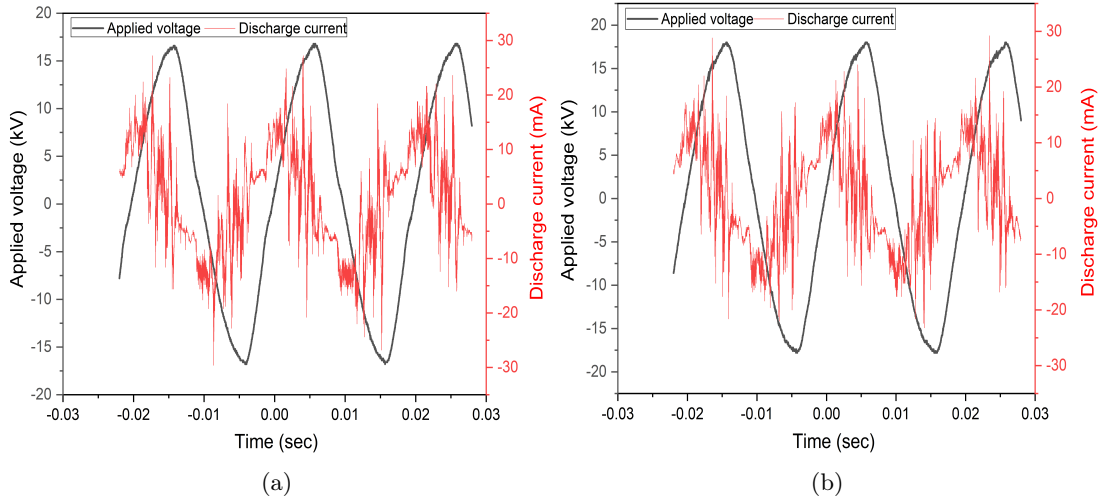


Figure 4: I(t)-V(t) signal of (a) air and (b) argon DBD.

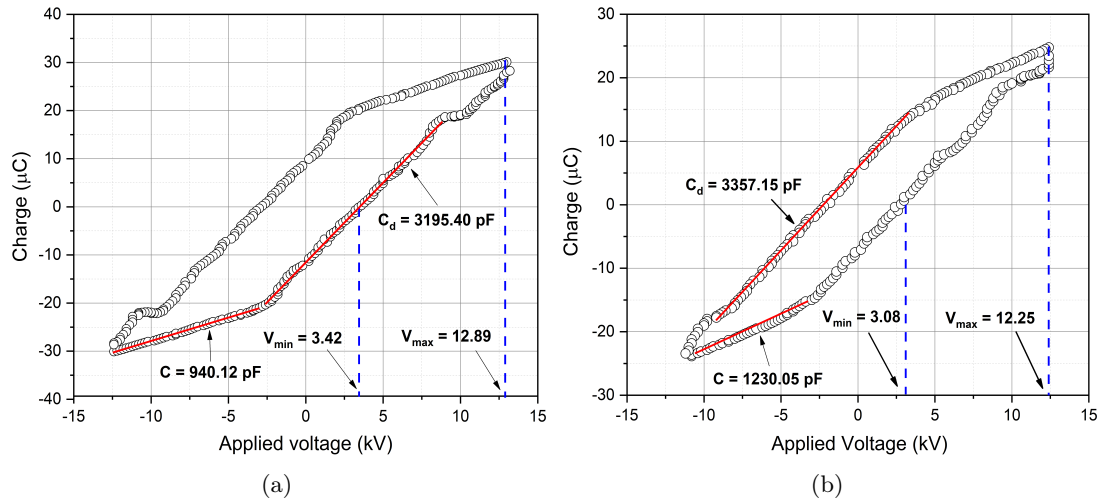


Figure 5: Lissajous figure of discharge in (a) air and (b) argon DBD .

Figures 5 show the Lissajous figure of DBD generated in the air and argon environment at the applied voltage of 15.65 kV with an air gap of 0.15 cm. The energy consumed per cycle is given by [22]:

$$E = 4C_d V_{min} \left(\frac{1}{1 + \frac{C_g}{C_d}} \right) (V_{max} - V_{min}) \quad (1)$$

And, the power dissipated is given by [23,24]:

$$P = 4f C_d V_{min} \left(\frac{1}{1 + \frac{C_g}{C_d}} \right) (V_{max} - V_{min}) \quad (2)$$

where, C_g = capacitance of air space, C_d = capacitance of the dielectric, V_{max} = maximum value of applied voltage required to initiate discharge, V_{min}

= minimum value of applied voltage, and f = frequency of input voltage.

In this study, the values of V_{max} , V_{min} , C , C_d , and C_g obtained from the Lissajous figure [Figure 5(a) and 5(b)] were found to be 12.89 kV, 3.42 kV, 940.12 pF, 3195.40 pF, and 1332.01 pF, respectively in the case of air environment, while they were found to be 12.25 kV, 3.08 kV, 1230.05 pF, 3357.15 pF, and 1941.36 pF, respectively, in the case of argon environment. With these values, the energy consumed per cycle was found to be 0.29 J and 0.24 J while the power dissipated was found to be 14.60 W and 12.00 W in the air and argon environments, respectively.

The average electron density (n_e) is calculated by [25]:

$$n_e = \frac{J_{av}}{eE\mu_e} \quad (3)$$

where, J_{av} = average current density, E = electric

field in the discharge region, and μ_e = electron mobility which is calculated with the help of BOLSIG+ software.

In the air environment, we found $J_{av} = 150.05$ mA/cm², $E = 16.07$ kV/cm, and $\mu_e = 335.12$ cm²/Vs. By substituting these values in equation (3), the average electron density (n_e) was estimated to be 1.74×10^{11} cm⁻³. Similarly, in the argon environment, we found $J_{av} = 180.34$ mA/cm², $E = 13.00$ kV/cm, and $J_{av} = 346.12$ cm²/Vs. By substituting these values in equation (3), the average electron density (n_e) was estimated to be 2.50×10^{11} cm⁻³.

3.3 Variation of power dissipated

Figure 6 shows the variation of power dissipated in the discharge in air and argon DBD at different applied voltages. It was found that as the applied voltage was increased, the power dissipated in air and argon DBD increased. This is because initially, available charged species are gaining energy from supplied voltages to cause further ionization of air and argon atoms [26]. At a particular applied voltage, the power dissipated in air DBD was found to be higher in comparison to argon DBD. Air plasma consists of about 78% nitrogen. Nitrogen being a diatomic molecule, its breakdown voltage is comparatively higher than argon in argon plasma [27].

3.4 Variation of average electron density

Figure 7 shows the variation of average electron density in air and argon DBD at different applied voltages. It was observed that when the applied voltage was increased, the average electron density was also found to be increased. This is because by increasing the voltage, the energy received by charge species also increases. As a result, kinetic energy rises, and the collisional mode shifts from elastic to inelastic. The emission of secondary electrons begins and will continue to increase as the applied voltage is increased [28].

Similarly, the average electron density in argon plasma was found to be higher in comparison to air plasma at the particular applied voltage, as the high number of argon atoms gets readily ionized, resulting in a stream of secondary electrons due to the relatively lower breakdown voltage of argon plasma in comparison to air plasma. Also in air plasma, a dissociative recombination process between electrons and ionized nitrogen molecules takes place [27, 29].

3.5 Optical Characterization

The line intensity ratio method has been used to estimate electron temperature [30, 31]:

$$\frac{R_1}{R_2} = \frac{\frac{I_1}{I_2}}{\frac{I_3}{I_4}} = \left(\frac{A_{pq}}{A_{rs}}\right) \left(\frac{g_p}{g_r}\right) \left(\frac{\lambda_{rs}}{\lambda_{pq}}\right) \left(\frac{A_{uv}}{A_{xy}}\right) \times \left(\frac{g_u}{g_x}\right) \left(\frac{\lambda_{xy}}{\lambda_{uv}}\right) \exp\left[-\frac{-E_p - E_r - E_x + E_v}{k_B T_e}\right] \quad (4)$$

where, λ is the wavelength of spectral lines, I is the intensity of spectral lines, A is the transition probability, g is the statistical weight and E is the energy of spectral lines.

a. Calculation of electron temperature in air DBD

Figure 8 shows the optical spectra of discharge in air plasma and corresponding values of intensity ranging from 300 to 460 nm at an applied voltage of 15.65 kV.

From the spectral lines of the discharge in air DBD, four suitable nitrogen lines - nitrogen first line NI (413.76 nm, 439.24 nm) and nitrogen second line NII (411.10 nm, 437.95 nm) were taken for electron temperature estimation. The NIST database is used to obtain the values of A_{ji} , g_i , and E_i for these four lines [32].

Table 1 shows the possible values of electron temperature and their corresponding intensity ratio values in the case of air DBD.

Figure 9 shows the variation of intensities ratio $\frac{R_1}{R_2}$ for different possible values of electron temperature. The four nitrogen lines taken have an intensities ratio equal to 1.03 which corresponds to an electron temperature of 1.31 eV.

b. Calculation of electron temperature in argon plasma

Figure 10 shows the optical spectra of discharge in argon plasma and corresponding values of intensity ranging from 300 to 900 nm at the applied voltage of 15.65 kV. From the spectral lines of the discharge in argon plasma, four suitable argon lines - argon first-line AI (696.02 nm, 750.38 nm) and argon second-line AII(336.65 nm, 356.32 nm) were taken for electron temperature estimation. The values of A_{ji} , g_i , and E_i for these four lines are obtained from the NIST database [32, 33].

Table 2 shows the possible values of electron temperature and their corresponding intensity ratios values of the spectral lines in the case of argon plasma.

Figure 11 shows the variation of intensities ratio $\frac{R_1}{R_2}$ for different possible values of electron temperature.

The four argon lines taken have an intensities ratio equal to 0.49 which corresponds to an electron temperature of 0.68 eV.

Table 1: Electron temperature (T_e) and intensity ratio.

Electron temperature (T_e)	Intensity Ratio ($\frac{R_1}{R_2}$)
0.80	13.44
0.90	7.06
1.00	4.21
1.20	1.94
1.40	1.12
1.60	0.74
1.80	0.54

Table 2: Electron temperature (T_e) and their corresponding intensity ratios.

Electron temperature (T_e)	Intensity Ratio ($\frac{R_1}{R_2}$)
0.60	1.88
0.65	0.78
0.70	0.37
0.80	0.11
0.90	0.04
1.00	0.02

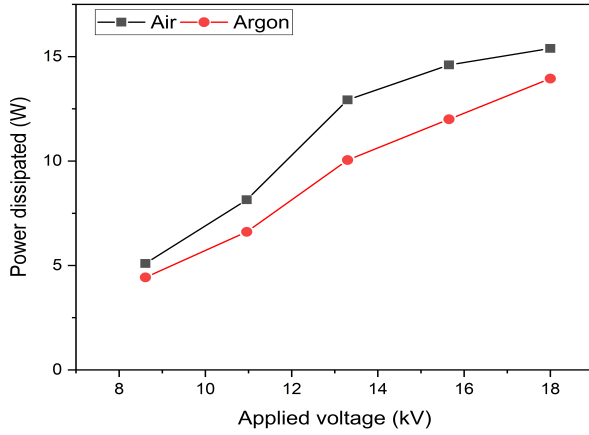


Figure 6: Variation of power dissipated at different voltages.

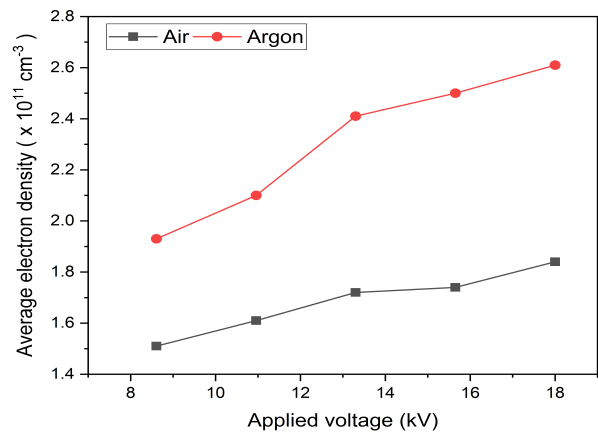


Figure 7: Variation of average electron density at different applied voltages.

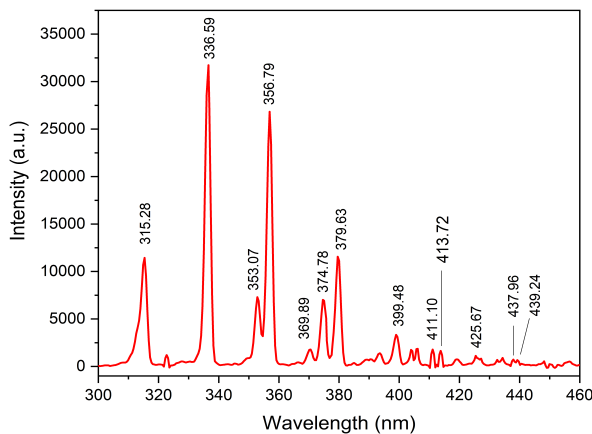


Figure 8: Optical emission spectra of discharge in air DBD.

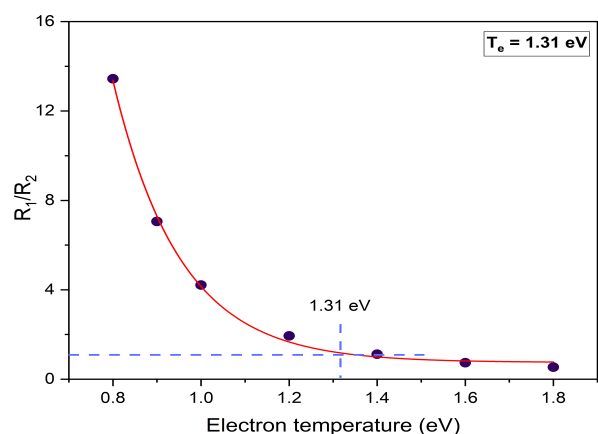


Figure 9: Variation of intensities ratio with electron temperature.

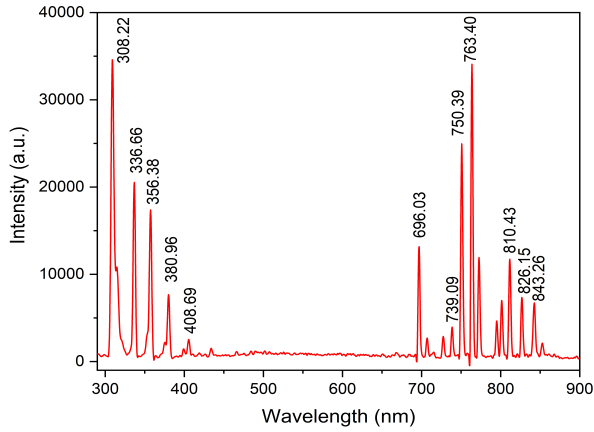


Figure 10: Optical emission spectra of discharge in argon DBD.

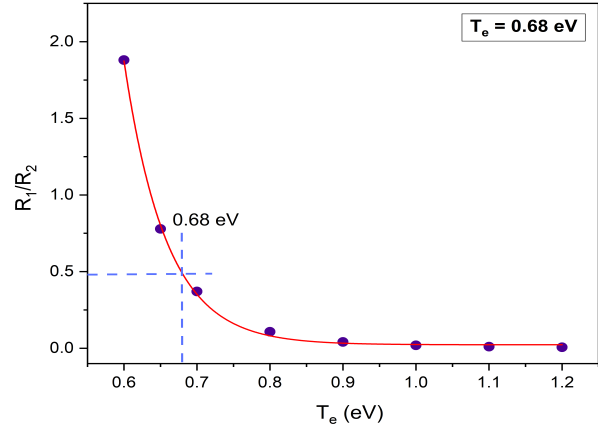


Figure 11: Variation of intensities ratio with electron temperature.

4 Surface Characterization

4.1 Mass loss (%)

To ensure the etching and deposition of the plasma ion process, mass loss (%) calculation was done given by [34]:

$$\text{Mass loss}(\%) = \left(\frac{M_i - M_f}{M_i} \right) \times 100 \quad (5)$$

where, M_i = initial mass of the sample before treatment and M_f = final mass of the sample after treatment.

A nylon 6 sample of dimension 2.5 cm × 2.5 cm was taken and its mass was measured in analytical balance (MG124Ai). Then, the sample was treated in air and argon DBD for a specified time and the mass of the treated sample was measured immediately after treatment.

Figures 12(a) and 12(b) show the mass loss (%) in the Nylon 6 sample after being treated in air and argon DBD for specified times. Initially, mass loss (%) was found to be increased on increasing the treatment time (from 5 to 15 minutes) in air DBD. Then, no significant difference in mass loss (%) was found between 15 and 20 minutes of treatment time. Initially, there was a 1.52% mass loss when the sample was treated for 1 minute in argon DBD. Then on further increase in treatment time, there was no significant difference in mass loss (%). This might be because once all the etchable materials have been removed from the surface, the remaining material is difficult to remove, resulting in a decrease in etching rates. The re-deposition of sputtered fragments could also contribute to the decline in etching rate [34, 35].

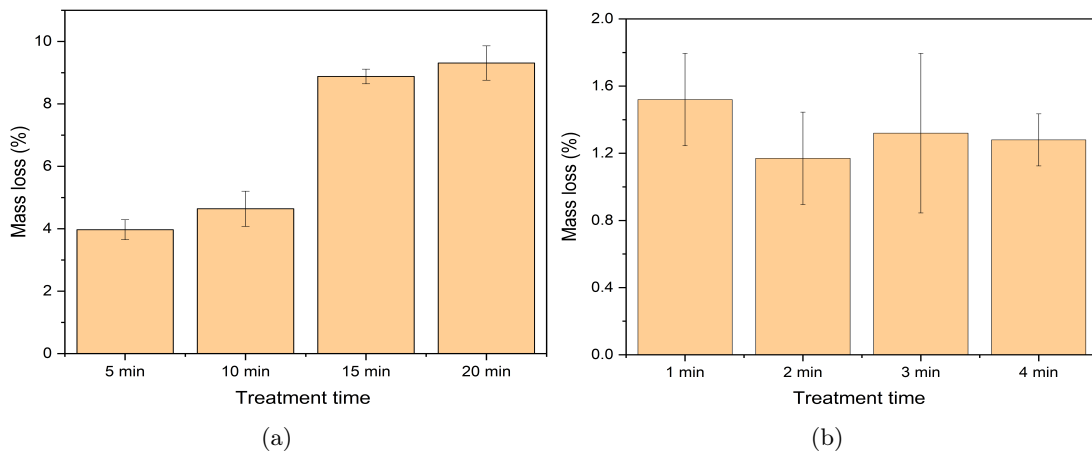


Figure 12: Mass loss (%) at different treatment times in (a) air and (b) argon DBD.

4.2 Water contact angle

A liquid's ability to wet a solid's surface is measured by the contact angle. It is the most important technique for studying the properties of a surface. The contact angle is the angle formed by a liquid at the three-phase boundary, where a liquid, gas, and solid meet [36,37].

The water contact angle is calculated using Young's equation for a perfect, uniform, and homogeneous surface at equilibrium [Figure 13] and is given by [38]:

$$\cos \theta = \frac{\gamma_{sv} - \gamma_{sl}}{\gamma_{lv}} \quad (6)$$

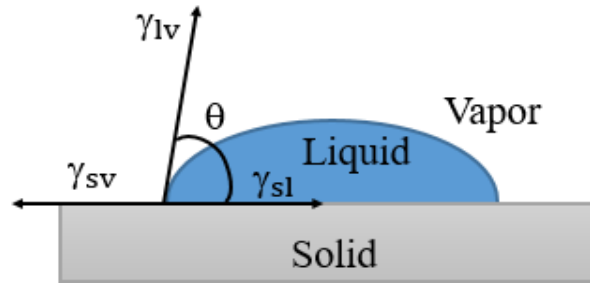


Figure 13: Schematic representation of Young's equation

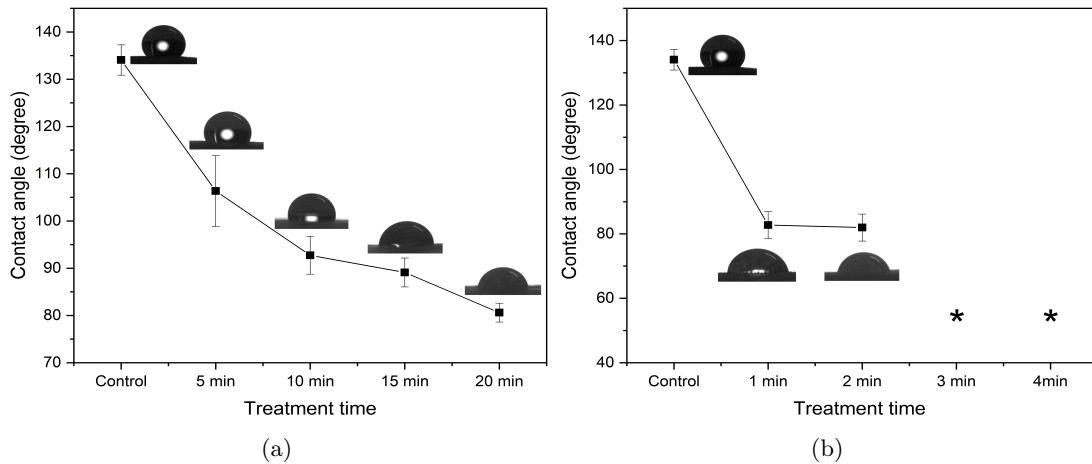


Figure 14: Water contact angle of the controlled and treated sample in (a) air and (b) argon DBD.

It was found that there was a decrease in water contact angle when the treatment time was increased in both air and argon plasma. The result shows that the sample became hydrophilic after being treated for 15 minutes in air DBD. Whereas, the sample became hydrophilic when treated for 1 minute in argon DBD. Moreover, the sample was completely wettable when treated for 3 minutes in argon DBD. The increase in the hydrophilicity of the sample after being treated in air and argon DBD could be because of the inclusion of hydrophilic groups such as CO, COOH, C-OH, -OH, etc [13–15, 39].

4.3 Surface free energy

The surface tension of a solid can be taken as a measure of surface-free energy. The behavior of any liquid on the surface may be predicted by knowing the solid's surface free energy. The surface free energy of solids from a single contact angle measurement of a liquid with a known surface tension is calcu-

lated by using the Kwok and Neumann equation and given by [40, 41]:

$$\gamma_l(1 + \cos \theta) = 2\sqrt{\gamma_s \gamma_l} [1 - \beta_l(\gamma_s - \gamma_l)^2] \quad (7)$$

where, $\beta_l = 0.0001057 (m^2/mJ)^2$.

Figure 15 shows the variation of surface free energy with treatment time in air and argon DBD respectively.

The surface free energy of the controlled sample was $(5.26 \pm 1.11) \text{ mJ/m}^2$. The surface free energy of the sample when treated in air DBD for 5 minutes, 10 minutes, 15 minutes, and 20 minutes were found to be $(19.23 \pm 4.31) \text{ mJ/m}^2$, $(27.52 \pm 2.51) \text{ mJ/m}^2$, $(29.78 \pm 1.91) \text{ mJ/m}^2$ and $(35.10 \pm 1.85) \text{ mJ/m}^2$ respectively. Similarly, the surface free energy of the sample when treated in argon plasma for 1 minute and 2 minutes were found to be $(33.77 \pm 2.63) \text{ mJ/m}^2$ and $(34.26 \pm 2.63) \text{ mJ/m}^2$ respectively. The result showed that the surface free energy of the sample increases as the treatment time is increased.

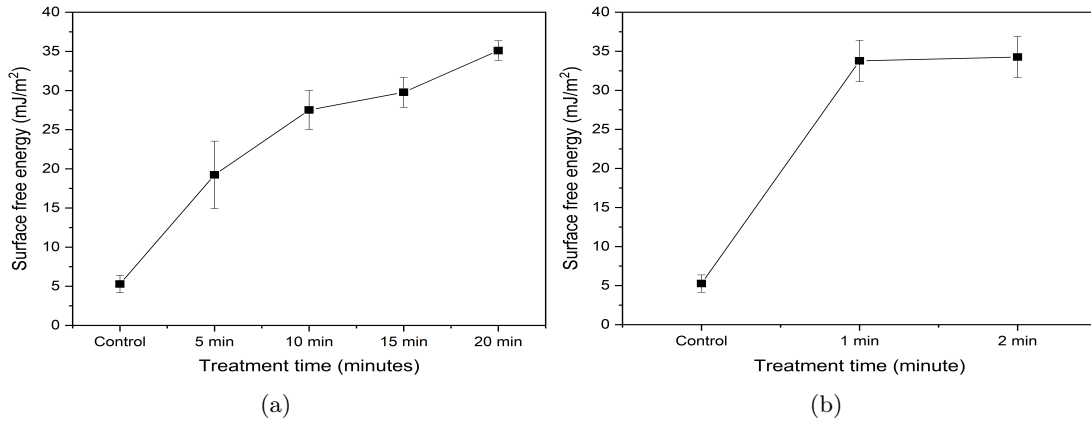


Figure 15: Variation of surface free energy with treatment time in (a) air and (b) argon DBD.

5 Conclusions

A custom-designed dielectric barrier discharge system operating at line frequency and at atmospheric pressure, utilizing air and argon as working gases, was used for surface modification of Nylon 6. The average electron density in both air and argon DBD was found to be in the order of 10^{11} cm^{-3} . The power dissipated and average electron density in the discharge were found to be increased on increasing the applied voltage in both air and argon DBD. At a particular applied voltage, the average density of electrons in argon DBD was found to be relatively higher in comparison to air DBD. In contrast, the temperature of electrons in air DBD was found to be comparatively higher than in argon plasma. The generated air and argon DBD significantly enhanced the hydrophilicity of Nylon

6, which was previously hydrophobic. In addition, the hydrophilicity and surface free energy of the sample was found to be increased by increasing the treatment time in both air and argon DBD. After 15 minutes of treatment with air DBD and 1 minute of treatment with argon DBD, the hydrophobic sample became hydrophilic. This shows that argon DBD is more effective than air DBD in the surface modification of Nylon 6. These findings have implications for the surface modification of other polymers and may have practical applications in industries such as medical devices and packaging.

Acknowledgments

The corresponding author was supported by the Nepal Academy of Science and Technology (NAST), Nepal through a Ph.D. fellowship. The authors

would also like to acknowledge all the researchers of the Plasma Physics Laboratory, Kathmandu University who provided valuable suggestions and help for the completion of this work.

References

- [1] Md Rabiul Rahman et al. Importance of sustainable polymers for modern society and development. *Advances in Sustainable Polymer Composites*, pages 1–35, 2021. doi.org/10.1016/B978-0-12-820338-5.00001-1
- [2] Xiaofang Jia, Margarita Herrera-Alonso, and Thomas J McCarthy. Nylon surface modification. part 1. targeting the amide groups for selective introduction of reactive functionalities. *Polymer*, 47(14):4916–4924, 2006. doi.org/10.1016/j.polymer.2006.05.038
- [3] M. S. B. Reddy, Deepalekshmi Ponnamma, Ruchi Choudhary, and Kishor Kumar Sadasivuni. A comparative review of natural and synthetic biopolymer composite scaffolds. *Polymers*, 13(7):1105, 2021. doi.org/10.3390/polym13071105
- [4] H. B. Baniya, R. P. Guragain, and D. P. Subedi. Cold atmospheric pressure plasma technology for modifying polymers to enhance adhesion: A critical review. In *Progress in Adhesion and Adhesives*, pages 841–879. 2021. doi.org/10.1002/9781119846703.ch19
- [5] Wei Zhang, L Johnson, SRP Silva, and MK Lei. The effect of plasma modification on the sheet resistance of nylon fabrics coated with carbon nanotubes. *Applied Surface Science*, 258(20):8209–8213, 2012. doi.org/10.1016/j.apsusc.2012.05.023
- [6] Fabienne Poncin-Epaillard et al. Surface treatment of polymeric materials controlling the adhesion of biomolecules. *Journal of Functional Biomaterials*, 3(3):528–543, 2012. doi.org/10.3390/jfb3030528
- [7] S. K. Nemani et al. Surface modification of polymers: Methods and applications. *Advanced Materials Interfaces*, 5(24):1801247, 2018. doi.org/10.1002/admi.201801247
- [8] R. P. Guragain et al. Improvement of hydrophilicity of polypropylene film by dielectric barrier discharge generated in air at atmospheric pressure. *Reviews of Adhesion and Adhesives*, 9(1):153–166, 2021.
- [9] G. Borgia, C. A. Anderson, and N. M. D. Brown. The surface oxidation of selected polymers using an atmospheric pressure air dielectric barrier discharge. part i. *Applied Surface Science*, 225(1-4):186–197, 2004. doi.org/10.1016/j.apsusc.2003.10.002
- [10] Y. Akishev, M. Grushin, V. Karalnik, D. Medvedev, N. Trushkin, A. Vasiliev, J. Schmitt, and K. D. Weltmann. Studies on cold plasma–polymer surface interaction by example of pp-and pet-films. *Journal of Physics D: Applied Physics*, 41(23):235203, 2008.
- [11] C. Feng, Y. Liu, W. Zheng, X. Yan, Z. Huang, and W. Cao. The effect of apgd plasma treatment on silk fabric. *Surface Engineering*, 36(5):485–491, 2020. doi.org/10.1080/02670844.2019.1609716
- [12] M. Laroussi, X. Lu, M. Keidar, and K. Ostrikov. Low temperature plasma-based sterilization: Overview and state-of-the-art. *Plasma Processes and Polymers*, 2(5):391–400, 2005. doi.org/10.1002/ppap.200400078
- [13] M. G. McCord et al. Modifying nylon and polypropylene fabrics with atmospheric pressure plasmas. *Textile Research Journal*, 72(6):491–498, 2002. doi.org/10.1177/004051750207200605
- [14] R.P. Guragain et al. Characterization of dielectric barrier discharge (dbd) produced in air at atmospheric pressure and its application in surface modification of high-density polyethylene (hdpe). *The Journal of Technological and Space Plasmas*, 1(1):27–35, 2020. doi.org/10.31281/jtsp.v1i1.11
- [15] R. Thompson, K. R. J. Lovelock, K. Potts, S. Thornthwaite, and K. K. Koziol. Low-frequency plasma activation of nylon 6. *Applied Surface Science*, 544:148929, 2021. doi.org/10.1016/j.apsusc.2021.148929
- [16] J. Lian, X. Jin, J. Jiang, S. Ye, X. Zhou, J. Zheng, and Z. Wang. Organocatalytic copolymerization of cyclic lysine derivative and -caprolactam toward antibacterial nylon-6 polymers. *ACS Macro Letters*, 11(1):46–52, 2021.
- [17] S. Kim, N. Lee, and J. Lee. Pyrolysis for nylon 6 monomer recovery from teabag waste. *Polymers*, 12(11):2695, 2020. doi.org/10.3390/polym12112695
- [18] F. F. Chen. *Introduction to plasma physics*. Springer Science & Business Media, 2012.
- [19] R. P. Guragain, H. B. Baniya, B. Shrestha, D. P. Guragain, and D. P. Subedi. Germination enhancement of mustard (*brassica nigra*) seeds using dielectric barrier discharge

- (dbd). *AIP Advances*, 13(3):035338, 2023. doi.org/10.1063/5.0146955
- [20] H. Jiang, T. Wang, Y. Liu, T. Shao, and J. Fang. Experimental study of qv lissajous figures in nanosecond-pulse surface discharges. *IEEE Transactions on Dielectrics and Electrical Insulation*, 20(4):1101–1111, 2013.
- [21] R. P. Guragain, H. B. Baniya, B. Shrestha, D. P. Guragain, and D. P. Subedi. Non-thermal plasma: A promising technology for the germination enhancement of radish (*raphanus sativus*) and carrot (*daucus carota sativus* l.). *Journal of Food Quality*, 2023:Article ID 4131657, 2023. doi.org/10.1155/2023/4131657
- [22] X. Tao, R. Lu, and H. Li. Electrical characteristics of dielectric-barrier discharges in atmospheric pressure air using a power-frequency voltage source. *Plasma Science and Technology*, 14(8):723, 2012.
- [23] T. C. Manley. The electric characteristics of the ozonator discharge. *Transactions of the Electrochemical Society*, 84(1):83, 1943.
- [24] R. P. Guragain et al. Growth enhancement of radish seed induced by low-temperature argon plasma. *Plasma Chemistry and Plasma Processing*, 43(1):111–137, 2023.
- [25] R. P. Guragain et al. Impact of non-thermal plasma treatment on the seed germination and seedling development of carrot (*daucus carota sativus* l.). *Journal of Physics Communications*, 5(12):125011, 2021.
- [26] G. D. Deepak, N. K. Joshi, U. Pal, and R. Prakash. Electrical characterization of atmospheric pressure dielectric barrier discharge-based cold plasma jet using ring electrode configuration. *Laser and Particle Beams*, 34(4):615–620, 2016. doi.org/10.1017/S0263034616000501
- [27] Phongsakorn Jitsomboonmit, Manop Nisoa, and Somsak Dangtip. Experimental study of current-voltage characteristics and optical emission of various gases in dielectric barrier discharge at atmospheric pressure. *Physics Procedia*, 32:723–731, 2012. doi.org/10.1016/j.phpro.2012.03.625
- [28] A. A. Khan, Y. S. Ling, and Z. Z. Chowdhury. Effect of varying voltage on electron density in oxygen homogenous dielectric barrier discharge under atmospheric pressure. *Malaysian Journal of Science*, 30(Sp3):10–20, 2019. doi.org/10.22452/mjs.sp2019no3.2
- [29] M. Moravej, V. M. Donnelly, A. R. Gibson, and R. Boswell. Physics of high-pressure helium and argon radio-frequency plasmas. *Journal of Applied Physics*, 96(12):7011–7017, 2004. doi.org/10.1063/1.1815047
- [30] N. Balcon, A. Aanesland, and R. Boswell. Pulsed rf discharges, glow and filamentary mode at atmospheric pressure in argon. *Plasma Sources Science and Technology*, 16(2):217, 2007.
- [31] H. B. Baniya et al. Generation and characterization of an atmospheric-pressure plasma jet (appj) and its application in the surface modification of polyethylene terephthalate. *International Journal of Polymer Science*, 2020, 2020.
- [32] Alexander Kramida, Yuri Ralchenko, John Reader, and NIST ASD Team. Nist atomic spectra database (version 5.10). *Online*, 2022. doi.org/10.18434/T4W30F
- [33] R. P. Guragain et al. Effect of plasma treatment on the seed germination and seedling growth of radish (*Raphanus sativus*). *Plasma Science and Technology*, 24(1):015502, 2021.
- [34] B. Paosawatyanong, K. Kamlangkla, and S. K. Hodak. Hydrophobic and hydrophilic surface nano-modification of PET fabric by plasma process. *Journal of Nanoscience and Nanotechnology*, 10(11):7050–7054, 2010. doi.org/10.1166/jnm.2010.2849
- [35] R. R. Deshmukh and N. V. Bhat. The mechanism of adhesion and printability of plasma processed PET films. *Materials Research Innovations*, 7:283–290, 2003. doi.org/10.1007/s10019-003-0265-z
- [36] Z. Shi et al. Dynamic contact angle hysteresis in liquid bridges. *Colloids and Surfaces A: Physicochemical and Engineering Aspects*, 555:365–371, 2018. doi.org/10.1016/j.colsurfa.2018.07.004
- [37] O. Ozkan and H. Y. Erbil. Interpreting contact angle results under air, water and oil for the same surfaces. *Surface Topography: Metrology and Properties*, 5(2):024002, 2017.
- [38] M. A. Q. Siddiqui et al. Current understanding of shale wettability: A review on contact angle measurements. *Earth-Science Reviews*, 181:1–11, 2018. doi.org/10.1016/j.earscirev.2018.04.002
- [39] A. Kuzminova et al. Study of the effect of atmospheric pressure air dielectric barrier discharge on nylon 6, 6 foils. *Polymer Degradation and Stability*, 110:378–388, 2014.

- doi.org/10.1016/j.polymdegradstab.2014.10.001
- [40] T. Zhang and T. Cui. Tunable wetting properties of patterned silicon microchannels with varied surface free energy based on layer-by-layer nano self-assembly. *Journal of Micromechanics and Microengineering*, 21(4):045015, 2011.
- [41] D. K. Owens and R. C. Wendt. Estimation of the surface free energy of polymers. *Journal of Applied Polymer Science*, 13(8):1741–1747, 1969. doi.org/10.1002/app.1969.070130815